Chemical Engineering Journal 93 (2003) 121–133

Chemical Engineering Journal

www.elsevier.com/locate/cej

Particle population balance model for a circulating fluidized bed boiler

Qinhui Wang*, Zhongyang Luo, Mingjiang Ni, Kefa Cen

Clean Energy and Environmental Engineering Key Lab of MOE, Institute for Thermal Power Engineering, Zhejiang University, 20 Yogu Road, Hangzhou 310027, China

Received 30 November 2001; accepted 25 August 2002

Abstract

A two-dimensional particle population balance model has been developed for the particle size and density distributions in a circulating fluidized bed (CFB) boiler furnace based on analysis of particle properties and the core–annulus hydrodynamic model. The model, incorporating modules to consider fuel particle fragmentation, char combustion, particle attrition and gas–solid separation, is part of an overall model developed earlier by the authors to simulate the operation of a 12 MW CFB boiler. The model predictions for particle population in a CFB furnace agree well with the measurement data.

Keywords: Circulating fluidized bed boiler; Particle population balance

1. Introduction

The complex hydrodynamics and char combustion behavior of circulating fluidized bed (CFB) boilers have not been fully understood. The properties and size distribution of particles have significant influence on the hydrodynamics and combustion behavior in the CFB furnace [1–3]. While a number of models of particle size distribution in fluidized beds have been reported, little is known of the particle size distribution in circulating fluidized bed boilers [4–9]. Most of the published models for the particle population balance in CFB boilers do not consider some important processes occurring in the furnace, such as char burning and attrition while the particles are traveling in the primary loop, particles with different properties undergo different physical and chemical processes. These previous models still have some limitations in describing the particle properties and population balance in the CFB boilers [7,8].

The present work is intended to develop a particle population balance model for circulating fluidized beds based on the experiments completed in a 12 MW CFB boiler, taking into account major physical and chemical processes that occur in CFB boilers.

2. Particle properties in CFB furnace

The solids inventory in a CFB furnace consists of spent and reacting fuel and sorbent particles and inert bed materials. The properties of feed particles have significant influence on the particle population balance in a CFB furnace. Additional bed material, like river sand, may be needed when a fuel with low ash content is fired. Even for a given fuel, properties such as the ultimate analysis may be subject to variations from time to time. In some cases, since the minerals content differs from particles to particle, a fuel sample may be divided into ash-rich and ash-lean portions [10]. Therefore, it is justified to assume that the proximate and ultimate analyses of a fuel sample represent the mean values of a distributed function for all particles present in the sample. Because the coal particles with different properties behave differently in the furnace, it is necessary to divide the feed particles into a number of groups with different proximate and ultimate analyses, e.g. with different ash contents.

Fuel particles (char) are assumed to consist of both reactive (carbon) and inert (ash) materials uniformly distributed throughout the reactive particle core. The reactivity of a particle undergoing gas–solid reactions in CFB boiler can be modeled by one of the three limiting types: (1) shrinking particle with a shrinking-core, i.e. the dual shrinking-core model; (2) constant sized particle with a shrinking-core, i.e. the classic shrinking-core model; and (3) uniform reaction model. In general, coal particles with high ash contents usually burns in a manner described by the dual shrinking-core model with changing size and density, while those with low

* Corresponding author. Tel.: +86-571-8795-2802; fax: +86-571-8795-1616.
E-mail address: qhwang@cmee.zju.edu.cn (Q. Wang).

1385-8947/02/$ – see front matter
PII: S1385-8947(02)00228-0

Nomenclature

A	cross-sectional area (m^2)
A_d	cross-sectional area of the dense bed (m^2)
C_i	ith particle component concentration (kg/m^3)
$CO_{2,\infty}$	oxygen concentration in the bed (kg/m^3)
d_p	sauter particle diameter (m)
D_{ac}	dispersion coefficient from the annulus to the core (m/s)
D_{ca}	dispersion coefficient from the core to the annulus (m/s)
D_h	diffusion coefficient of oxygen in the ash shell (m^2/s)
D_l	axial dispersion coefficient (m^2/s)
D_{spi}	ith particle component of axial dispersion coefficient in the cyclone (m^2/s)
D_t	furnace equivalent diameter (m)
E_i	initial entrainment rate of particle group i (kg/m^2 s)
f	mass fraction of solid particle
f_s	ratio of weight consumption of char to that of oxygen
F	interface between the core and the annulus (m)
F_0	mass flow rate of feed (kg/s)
F_{d2}	bed material drain rate (kg/s)
F_{d2}	mass flow rate of back down the dense bed from the dilute region (kg/s)
F_{in}	recycle solids rate (kg/s)
$F_{in,i}$	ith mass component flowing into the cell (kg/s)
$F_{out,i}$	ith mass component flowing out of the cell (kg/s)
F_{u1}	mass flow rate of elutriated into the dilute region (kg/s)
g	gravitational acceleration (m/s^2)
G_{ai}	generating rate of i particle in the annulus (kg/s)
G_{ci}	generating rate of i particle in the core (kg/s)
G_{spi}	generating rate of particle group i in the cyclone (kg/s)
h	height above the distributor (m)
H	furnace height (m)
k_a	attrition constant
k_c	chemical reaction rate constant (m/s)
k_f	fragmentation constant
k_s	specific combustion rate of char particle (kg/m^2 s)
l	length of the spiral in the cyclone (m)
m	mass of solid particle (kg)
M_1	bed material inventory in the dense bed (kg)
M_a	bed material inventory in the annulus (kg)
M_c	bed material inventory in the core region (kg)
$P(R, \rho)$	particle mass distribution function
$P_0(R, \rho)$	particle mass distribution function of feed mass flow
$P_1(R, \rho)$	particle mass distribution function of the bed inventory
$P_{d1}(R, \rho)$	particle mass distribution function of drained bed material
$P_{d2}(R, \rho)$	particle mass distribution function of mass flow that back down the dense bed
$P_f(R)$	normal size distribution
$P_{in}(R, \rho)$	particle distribution function of recycle solids
$P_{new}(d_p,\text{new})$	size distribution after fragmentation
$P_{old}(d_p,\text{new})$	size distribution before fragmentation
$P_{u1}(R, \rho)$	particle mass distribution function of mass flow that elutriated into dilute region
r	particle radius (m)
R	particle diameter (m)
R_a	particle attrition rate (kg/s)
R_{a0}	particle attrition rate in the steady-state (kg/s)
Re	Renault number
R_f	upper size limit of the fines produced by attrition (m)
R_m	maximum particle diameter (m)

R_l	radius of char particle (m)
S_{ai}	feed rate per meter height of particle group i in the annulus (kg/s)
S_{ci}	feed rate per meter height of particle group i in the core (kg/s)
t	time (s)
U	gas velocity (m/s)
U_0	superficial gas velocity (m/s)
U_{gc}	gas velocity in the core (m/s)
U_{mf}	minimum fluidization velocity (m/s)
V_t	particle terminal velocity (m/s)
V	particle velocity (m/s)
V_{pi}	ith component of particle velocity (m/s)
V_{sl}	slip velocity between the gas velocity and the upward particle velocity (m/s)
W_b	mass of particle in the furnace (kg)
Z	height (m)

Greek symbols

β_0	mass transfer coefficient (m/s)
δ	thickness of annulus (m)
ϵ_{mf}	bed voidage at minimum fluidization
ζ	thickness of the ash shell (m)
μ	mean value of normal distribution function
μ_g	gas viscosity (kg m^{-1} s^{-1})
ρ	average particle density (kg/m^3)
ρ_1	density of char particle core (kg/m^3)
ρ_2	density of ash shell (kg/m^3)
ρ_s	solid particle density (kg/m^3)
ρ_{max}	maximum solid particle density in the furnace (kg/m^3)
ρ_{min}	minimum solid particle density in the furnace (kg/m^3)
σ	standard deviation of normal distribution function
$\phi(x)$	cumulative normal distribution function

Subscripts

i	particle size increment
c	core
a	annulus

ash contents tend to follow the shrinking-core model with no surrounding ash layer. For the fine particles under kinetic control, volume reaction is usually assumed. These three reaction modes may occur simultaneously within a CFB boiler furnace, with different particles obeying different models.

Since particles with the same diameter may have different carbon contents and therefore, different densities, a particle population balance should be described in terms of a distributed particle size and density. The particle mass distribution functions may be given as $P(R, \rho)$. A char particle in a CFB boiler is illustrated in Fig. 1. The average particle density, ρ, is a function of the reduced core radius, R_c/R, and the densities of the core and ash layer, denoted as ρ_1 and ρ_2, respectively

$$\rho = (\rho_1 - \rho_2)\left(\frac{R_c}{R}\right)^3 + \rho_2. \quad (1)$$

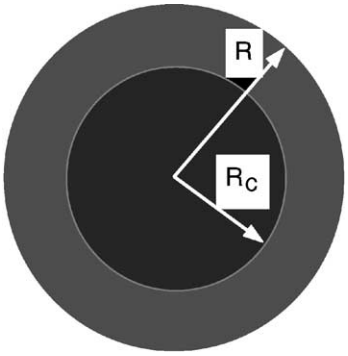

Fig. 1. Schematic of a reacting particle.

It is assumed that the rate of change in the particle radius is determined only by attrition, while the rate of change in the particle density is determined by both attrition and combustion reactions

$$\frac{\partial R}{\partial t} = \left.\frac{\partial R}{\partial t}\right|\text{att} = \frac{R}{3m}R_a, \tag{2}$$

$$\frac{\partial \rho}{\partial t} = \left.\frac{\partial \rho}{\partial t}\right|\text{rea} + \left.\frac{\partial \rho}{\partial t}\right|\text{att}, \tag{3}$$

where $(\partial R/\partial t)|$att is the particle shrinking rate due to attrition (in m/s). $(\partial \rho/\partial t)|$rea is the rate of change in particle density due to reaction (in kg/(m^3 s)), $(\partial \rho/\partial t)|$att is the term due to attrition.

3. Particle population balance model

It has been widely accepted that a CFB furnace may be characterized by two flow regimes: a dense bed at the bottom and a dilute region above the solid entry or secondary air inlet. Because there are great differences in the hydrodynamics between the dense bed and the dilute region, the particle population models for the two respective regimes should be developed separately.

3.1. Particle population balance for dense bed

The dense bed operates in the turbulent fluidization regime. It may be assumed that the voidage in the dense bed is uniform. The solids mass balance in this region is given in Fig. 2. Here, M_1 is the inventory of the bed materials. F_0, F_{d1}, F_{u1}, F_{d2} and F_{in} are mass flow rates of feed, bed drain, particles entrained into the dilute region, mass reflux into the dense bed and recycled solids, respectively. $P_0(R, \rho)$, $P_1(R, \rho)$, $P_{d1}(R, \rho)$, $P_{u1}(R, \rho)$, $P_{d2}(R, \rho)$, $P_{in}(R, \rho)$ represent, respectively, mass distribution function of solid particle range (R, ρ) in feed, dense bed, bed drain, entrainment, reflux and recycled solids. Based on previous researches [4,6,9], a particle population balance has been developed in the present work by proper accounting of attrition and reaction in the furnace. A number of studies [4,11,12] have shown that there are no intermediate-sized particles between the son particles and the fines produced from the particles attrition in fluidized beds. It is assumed that a mother particle undergoes attrition until it reaches the upper size limit of the fines produced from attrition, R_f, and then becomes a fine particle itself. The fines generated react further but not subject to further attrition. The particle size distribution is thus divided into two size ranges: one is from 0 to R_f for fines, and the other from R_f to the maximal size of feed particles R_m for mother particles. By considering the population of a given size (R, ρ), the solids mass balance for the mother particles is obtained

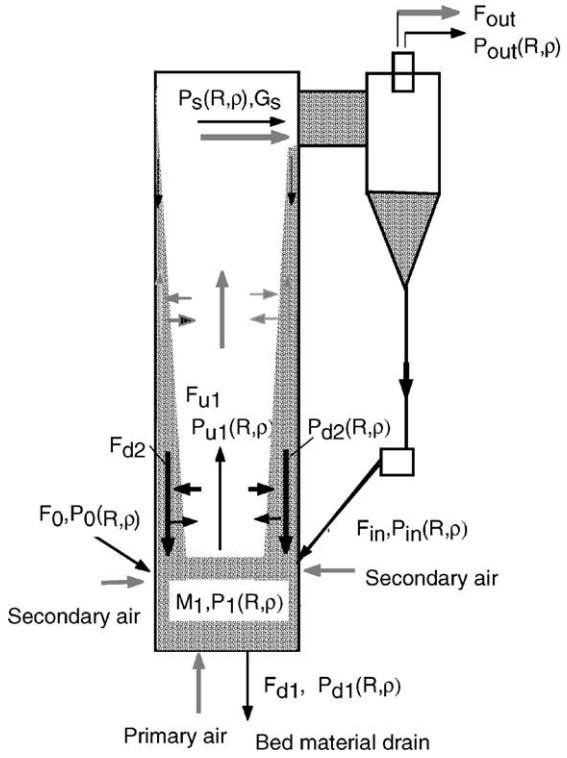

Fig. 2. Gas–solid flow structure and particle population balance in a CFB boiler.

$$\begin{aligned} &F_0P_0(R,\rho) - F_{d1}P_{d1}(R,\rho) - F_{u1}P_{u1}(R,\rho) + F_{d2}P_{d2}(R,\rho) \\ &\quad + F_{in}P_{in}(R,\rho) + M_1\frac{\partial P_1(R,\rho)}{\partial R}\frac{dR}{dt} + M_1\frac{\partial P_1(R,\rho)}{\partial \rho}\frac{d\rho}{dt} \\ &\quad - M_1P_1(R,\rho)\left(\frac{3}{R}\frac{dR}{dt} + \frac{1}{\rho}\frac{d\rho}{dt}\right) = 0 \end{aligned} \tag{4}$$

It is assumed that the fines generated from attrition of the mother particles have a size distribution (natural grain size) $P_f(R)$ independent of the volume scale [4]. Therefore, in the fine particle size region $(R_f \geq R > 0)$, population equation can be rewritten as

$$\begin{aligned} &F_0P_0(R,\rho) - F_{d1}P_{d1}(R,\rho) - F_{u1}P_{u1}(R,\rho) + F_{d2}P_{d2}(R,\rho) \\ &\quad + F_{in}P_{in}(R,\rho) + M_1\frac{\partial P_1(R,\rho)}{\partial R}\frac{dR}{dt}U_f(R_f) \\ &\quad + M_1\frac{\partial P_1(R,\rho)}{\partial \rho}\frac{d\rho}{dt} - M_1\frac{P_1(R,\rho)}{\rho}\frac{d\rho}{dt} \\ &\quad + \int_{R_f}^{R_m}\left[\frac{3M_1P(R,\rho)(dr/dt)|\text{att}}{r}\right]dr\,P_f(R) = 0. \end{aligned} \tag{5}$$

Here, U_f is a unit filter function, defined as

$$U_f(R) = \begin{cases} 1, & R = R_f, \\ 0, & R \neq R_f. \end{cases} \tag{6}$$

The last term in Eq. (5) represents the intake of the fines through attrition of the mother particles.

In addition, Eqs. (4) and (5) are subject to the following boundary conditions

$$\begin{cases} P_1(R,\rho) = 0, & R > R_m,\ R < 0 \text{ and} \\ & \rho \text{ outside the possible range}, \\ \int_0^{R_m}\int_{\rho_{min}}^{\rho_{max}} P_1(R,\rho)\,d\rho\,dR = 1. \end{cases} \tag{7}$$

3.2. Particle population balance for dilute region

The core–annulus flow structure in a CFB riser with circular or square cross-section is widely accepted. It may be assumed that particles travel upward in the core region and downward in the annulus, and there are no radial suspension density gradients within the core or annulus. The mass balance in differential form for group i particles can be written

$$\frac{\mathrm{d}(V_{ci}C_c f_{ci}A_c)}{\mathrm{d}Z} = \frac{\mathrm{d}}{\mathrm{d}Z}\left[A_c D_{lci}\frac{\mathrm{d}(C_c f_{ci})}{\mathrm{d}Z}\right] + S_{ci} + G_{ci}. \quad (8)$$

for the core region and

$$\frac{\mathrm{d}(V_{ai}C_a f_{ai}A_a)}{\mathrm{d}Z} = \frac{\mathrm{d}}{\mathrm{d}Z}\left[A_a D_{lai}\frac{\mathrm{d}(C_a f_{ai})}{\mathrm{d}Z}\right] + S_{ai} + G_{ai}. \quad (9)$$

for the annulus.

There is solids exchange between the core and the annulus. The net mass exchange rate can be treated as a source term for each region. For the core region, the feed rate of group i particles over unit riser height, S_{ci}, is given as

$$S_{ci} = (D_{aci}C_a f_{ai} - D_{cai}C_c f_{ci})F. \quad (10)$$

Similarly, for the annulus

$$S_{ai} = (D_{cai}C_c f_{ci} - D_{aci}C_a f_{ai})F. \quad (11)$$

Over a particle size interval from R to $R+\Delta R$ and density interval from ρ to $\rho+\Delta\rho$, the balances for group i particles with radius R and density ρ should include the following terms: (i) solids entering this size grade from the next larger size grade by attrition; (ii) solids leaving this grade by attrition; (iii) solids entering this density grade from the next larger density class due to reaction and/or attrition; (iv) solids leaving this grade due to reaction and/or attrition; and (v) solids in the grade which undergo reaction and attrition but staying in the current size and density intervals.

Accordingly, the generation rate of group i particles within the increments ΔR and $\Delta\rho$ in the core region, G_{ci}, is determined by the attrition rate and the combustion rate

$$\begin{aligned}
G_{ci} &= G_c(R,\rho)\\
&= M_c P_c(R,\rho)\frac{\partial\rho}{\partial t}\Delta R|_{R,\rho+\Delta\rho} - M_c P_c(R,\rho)\frac{\partial\rho}{\partial t}\Delta R|_{R,\rho}\\
&\quad + U_{f1}(R_m,R_f)M_c P_c(R,\rho)\frac{\partial R}{\partial t}\Delta\rho|_{R+\Delta R,\rho}\\
&\quad - U_{f1}(R_m,R_f)M_c P_c(R,\rho)\frac{\partial R}{\partial t}\Delta\rho|_{R,\rho}\\
&\quad - M_c P_c(R,\rho)\Delta R\Delta\rho\\
&\quad \times\left(\frac{3(\mathrm{d}R/\mathrm{d}t)U_{f1}(R_m,R_f)}{R} + \frac{(\mathrm{d}\rho/\mathrm{d}t)}{\rho}\right)\\
&\quad + U_{f1}(R_f,0)\int_{R_f}^{R_m}\left[\frac{3M_c P_c(R,\rho)(\mathrm{d}r/\mathrm{d}t)|_{\mathrm{att}}}{r}\right]\\
&\quad \times \mathrm{d}r\, P_f(R)\Delta R\Delta\rho. \qquad (12)
\end{aligned}$$

Similarly, G_{ai} for the annulus can be given as

$$\begin{aligned}
G_{ai} &= G_a(R,\rho)\\
&= M_a P_a(R,\rho)\frac{\partial\rho}{\partial t}\Delta R|_{R,\rho+\Delta\rho} - M_a P_a(R,\rho)\frac{\partial\rho}{\partial t}\Delta R|_{R,\rho}\\
&\quad + U_{f1}(R_m,R_f)M_a P_a(R,\rho)\frac{\partial R}{\partial t}\Delta\rho|_{R+\Delta R,\rho}\\
&\quad - U_{f1}(R_m,R_f)M_a P_a(R,\rho)\frac{\partial R}{\partial t}\Delta\rho|_{R,\rho}\\
&\quad - M_a P_a(R,\rho)\Delta R\Delta\rho\\
&\quad \times\left(\frac{3(\mathrm{d}R/\mathrm{d}t)U_{f1}(R_m,R_f)}{R} + \frac{(\mathrm{d}\rho/\mathrm{d}t)}{\rho}\right)\\
&\quad + U_{f1}(R_f,0)\int_{R_f}^{R_m}\left[\frac{3M_a P_a(R,\rho)(\mathrm{d}r/\mathrm{d}t)}{r}\right]\\
&\quad \times \mathrm{d}r\, P_f(R)\Delta R\Delta\rho. \qquad (13)
\end{aligned}$$

Here, U_{f1} is another unit filter function, defined as

$$U_{f1}(R_1,R_2) = \begin{cases} 1, & R_1 \geq R > R_2,\\ 0, & \text{elsewhere.}\end{cases} \quad (14)$$

The thickness of the annulus, δ, is correlated by Werther [13]

$$\frac{s}{D_t} = 0.55Re^{-0.22}\left(\frac{H_t}{D_t}\right)^{0.21}\left(\frac{H_t-h}{H_t}\right)^{0.73}. \quad (15)$$

The upward particle velocity in the dilute core region can be taken as

$$V_{ci} = U_{gc} - V_{sli}. \quad (16)$$

Plasynski et al. [14] reviewed correlations for predicting the particle velocity in a fast fluidized bed and used three indicators to evaluate the accuracy: the square of the deviation, the average absolute deviation and the standard deviation. It is indicated that if the slip velocity is taken equal to the terminal velocity, the calculated particle velocity shows better accuracy. Therefore, the particle slip velocity V_{sli} may be approximated by the terminal velocity of group i particles, V_{ti}. The gas velocity in the core, U_{gc}, is given by Bai et al. [15].

It is assumed that the downward solids velocity in the annulus is maintained constant, about 1.2–1.5 m/s [16,17]. The dispersion coefficients D_{lci}, D_{lai}, D_{aci}, D_{cai} can be obtained from previous literature [15,18–20]. Solving Eqs. (8) and (9) with the above expressions for G_{ci} and G_{ai}, the concentration and mass distribution density of group i particles in the core and the annulus can be obtained.

4. Models for the related processes

4.1. Fragmentation of coal particles

Previous studies suggested that primary fragmentation of coal particles in a fluidized bed occurred within a few seconds after injection of the particles into the bed due

to build-up of thermal and devolatilization-induced stresses [7,9]. It may be assumed that primary fragmentation occurs primarily in the zones close to the feed ports. An empirical correlation was proposed by Bellgardt et al. [9]

$$P_{\text{new}}(d_{\text{p,new}}) = P_{\text{old}}(d_{\text{p,new}}k_{\text{f}}^{-1/3})k_{\text{f}}^{1/3}. \quad (17)$$

Bellgardt et al. [9] suggest that the fragmentation constant k_{f} falls between 1 and 2 for a bubbling fluidized bed. Because of the higher superficial gas velocity, fragmentation in a CFB may have more pronounced effects on chemical reaction than in a bubbling fluidized bed.

4.2. Char combustion

The main assumptions for char combustion are: (i) both CO and CO_2 are primary products; (ii) CO burns after leaving the char particle surface; (iii) coal particles with high ash content burn according to the dual shrinking-core model, while for those with low ash content, single shrink-core model applies, and for fine particles, uniform reaction model should be employed; (iv) the combustion rate of char particles is determined by reaction kinetics, gaseous and intra-particle diffusion resistance's.

Based on the previous work [21], the specific combustion rate of a char particle, k_{s}, can be determined by

$$k_{\text{s}} = \frac{f_{\text{s}}\text{CO}_{2,\infty}}{(1/k_{\text{c}}) + (1/\beta_0)(R/R_1)^2 + (\zeta/D_{\text{h}})(R/R_{\text{c}})}, \quad (18)$$

where f_{s} is the ratio of mass consumption of char to that of oxygen, taking the values 0.375 and 0.75 for CO_2 and CO, respectively. ζ represents the thickness of the ash layer (in m); $\zeta = R - R_{\text{c}}$.

4.3. Particle attrition

In fluidized beds, particle attrition takes place by surface abrasion, i.e. particles of a much smaller size break away from the original particle. The upper limit size of the fines produced is in the range 50–100 μm [4,11,12].

The attrition rate is influenced by many factors including particle properties, solids concentration, particle size, residence time, particle temperature and superficial gas velocity. However, particle properties and gas velocity may have more great influences [4,22–24].

The attrition rate R_{a} is defined as

$$R_{\text{a}} = \frac{\text{d}m}{\text{d}t}. \quad (19)$$

Previous studies [4,11,12,24] show that fresh feed particles usually have an initial period of rapid attrition before the attrition rate slows down to a steady level. Ray et al. [4] carried out particle attrition experiments in a fluidized bed using limestone particles with a size range 300–1000 μm. Both the initial and steady-state attrition rates for the sample particles of the same mass and size under various fluidizing velocities were measured. The experiments indicated that fresh particles approach the steady-state attrition condition after approximately 3–5 wt.% of the original mass is stripped away. Pis et al. [11] carried out their experiments in a cold fluidized bed using coal ash particles. The coal ash used comes from a fluidized bed combustor. Three size ranges were used in the experiments: 0.2–0.315, 0.315–0.5 and 0.5–1 mm. The experiments under various superficial gas velocity and bed depth showed the particle attrition reached the steady-state between 3 and 4% of the mass stripped away. Because the mass fraction of the fresh feed particles in the CFB furnace is very small while most particles are more or less aged, the attrition rates of most particles in the furnace may be treated as the steady-state attrition rate.

According to a previous investigation [22], the steady-state attrition rate in a fluidized bed combustor may be given as

$$R_{\text{a0}} = k_{\text{a}}(U_0 - U_{\text{mf}})\frac{W_{\text{b}}}{d_{\text{p}}}. \quad (20)$$

Arena et al. [23] suggested that the above equation may be extended to char particle attrition during CFB combustion using the loads of group i particles in the furnace and their Sauter diameter. The attrition constant k_{a} is a function of solid mass flux and gas velocity in the furnace. The k_{a} value for CFB combustion is usually one to four times that for fluidized beds.

The particle attrition rate differs significantly between the dense bed and the upper dilute region in a CFB furnace due to different hydrodynamic properties. It can be expected that the attrition constant k_{a} for the dense bed is large due to the high solids concentration and violent particle collision, while k_{a} for the upper dilute region (including both the core and annulus) is much smaller due to the lower solid concentration and less frequent particle collision. In the present study, the attrition constant is determined based on data reported in previous literature.

There are several particulate materials in the CFB boiler furnace, each having its own attrition characteristics. Therefore, different attrition constants should be assigned to different components. Based on attrition characteristics, the particles in a CFB boiler can be divided into two types: particles with low ash content, and particles with high ash content. The attrition of inert particles can be neglected because they are independent of the chemical conversion process.

Because of its low mechanical strength, the ash layer of an ash-lean char particle is assumed to wear out immediately after it is formed during combustion. In addition, the ash-lean particles often undergo combustion-assisted attrition with faster attrition rate. Arena et al. [23] carried out char attrition experiments in a circulating fluidized bed combustor using char particles obtained by devolatilizing a South African bituminous coal with an ash content of 16.23%. The attrition constants obtained varied in the range $2–7 \times 10^{-7}$ with a superficial gas velocity of 4–6 m/s and a circulating solids mass flux from 100 to 200 $\text{kg/m}^2\,\text{s}$.

On the other hand, the mechanical strength of the ash layer of ash-rich char particles is higher than that of the ash-lean particles. Therefore, it can be assumed that only the ash layer is worn out as the particle undergoes reactions following a dual shrinking-core model. It is observed that a coarse ash particle drained from the bottom of a CFB boiler has an unburnt carbon core wrapped by a spent ash layer. This indicates that only the ash layer of such particles is gradually worn out by attrition in the furnace. The attrition constant k_a of the ash-rich particles is therefore lower than that of the ash-lean ones. Pis et al. [11] suggested a value of $k_a = 1.6 \times 10^{-7}$ for the attrition constant fitted to their experimental data of the coal ash particles in a fluidized bed. As an approximation, Eq. (20) may be used to determine the attrition rate of limestone particles.

4.4. Particles ejected from the dense bed

The rate of the particles ejected from the dense bed into the dilute region is a function of particle population density and gas velocity, i.e.

$$F_{u1i} = F_{u1} P_{u1}(R, \rho) = E_i A_d P_1(R, \rho). \quad (21)$$

Pemberton and Davidson [24] proposed the initial entrainment rate for group B particles with $U_0/U_{mf} > 10$–15

$$E_i = 0.1\rho_s(1 - \varepsilon_{mf})(U_0 - U_{mf}). \quad (22)$$

For coarse bed materials with a poly-dispersed size distribution commonly used in CFB boilers, Yan and co-workers [25] measured the entrainment rate in a fluidized bed cold model with 350 mm × 900 mm cross-section. The ash particles were sized from 0 to 13 mm, collected from a coal-fired fluidized bed boiler. The following empirical correlation was obtained from the experimental data

$$E_i = 0.6347\rho_g(U_0 - V_t)\left(\frac{U_0 - V_t}{V_t}\right)^{0.9649} \times \left[\frac{(U_0 - V_t)^2}{g d_p}\right]^{-0.2764}\left(\frac{d_p V_t \rho_g}{\mu_g}\right)^{0.4911}. \quad (23)$$

4.5. Model for the gas–solid separator

The gas–solid separator is a key component of the CFB boiler. Among different types, cyclones are the most commonly used separators in CFB boilers. The performance of the cyclone plays a significant role in determining the particle population balance in a CFB boiler. In the present study, a simplified model is developed to simulate the gas–solid flow structure in the cyclone. The main assumptions are: (i) Gas and solids move con-currently in plug flow around a helical path in the cyclone body; (ii) the cross-sectional area of the spiral is the same as that of the cross-sectional area at the entry point of the cyclone, and the gas–solid slip velocity entering the cyclone also depends on the entry area of the cyclone; (iii) gas–solid separation takes place only at the end of the spiral; (iv) the combustion of char and combustible gases also takes place in the cyclone due to the rapid mixing between the gas and solid phases.

Mass balance for each group of solid particles gives

$$\frac{d(V_{pi} C_i)}{dl} = D_{spi}\frac{d^2 C_i}{dl^2} + G_{spi}. \quad (24)$$

Classical models for the grade efficiency and overall separation efficiency are used to predict cyclone performance.

Table 1
Model input data

Parameter	Value
Rated capacity (T/h)	73
Main steam pressure (MPa)	3.82
Main steam temperature (°C)	450
Feed water temperature (°C)	105
Ambient air temperature (°C)	25
Combustion air flow (N m^3/h)	70,500
Primary air flow (N m^3/h)	42,000
Primary air ratio (%)	60

5. Model validation

The overall mathematical model of the CFB boiler has been developed by combining the above-discussed models together with sub-models for other physical and chemical processes [26,27]. The overall model is used to predict the performance of a 12 MW CFB boiler. The bituminous coal-fired boiler is the first of the type operational in China, which employs an external heat exchanger developed by Zhejiang University. The furnace is 21 m high and has a square cross-section measuring 5.45 m × 2.45 m in the membrane-wall covered region and 1.5 m × 5.45 m in the bottom refractory-lined section. Secondary air

Table 2
Analysis of test coal

Ultimate analysis, air dried basis	Value	Proximate analysis, air dried basis	Value
C_{ad}, carbon (wt.%)	63.01	$M_{t,ar}$, moisture, as-received (wt.%)	5.72
H_{ad}, hydrogen (wt.%)	3.59	M_{ad}, moisture (wt.%)	1.43
O_{ad}, oxygen (wt.%)	6.23	A_{ad}, ash (wt.%)	23.74
N_{ad}, nitrogen (wt.%)	1.15	V_{ad}, volatile matter (wt.%)	24.1
S_{ad}, sulfur (wt.%)	0.85	Q_{ad}, calorific value (MJ/kg)	24.45

Table 3
Particle size distribution of test coal

Diameter (mm)	0–0.1	0.1–0.3	0.3–0.5	0.5–1	1–1.5	1.5–2.0	2.0–3.5	3.5–5.0	5–6.5	6.5–8
Mass fraction (%)	0.5	2	6	16	9	10	13	18	12	13.5

inlets are located at 1.5, 2.0 and 2.5 m above the distributor in the two sidewalls. Oriented air nozzles are used to fluidize the bed and make the bottom ash move toward two draining holes at the backside of the furnace. Two cyclones with a diameter of 3 m are located at the furnace exit. The designed entrance-gas velocity is 25 m/s. Part of the solid particles separated by the two cyclones is cooled by the EHE, while the rest is recycled into the furnace by a pair of recycle devices. The flue gas from the two cyclones flows through the high-temperature superheater above the furnace, the low-temperature superheater, finned-tube economizer and tubular air preheater located in the backpass.

Particles in the furnace are divided into 70 different groups, i.e. 10 size groups from 0 to 8 mm and seven density intervals from 1100 to 2400 kg/m^3. Particles of each group are denoted by their mean diameters and densities.

Since most of the particles in the dilute region fall in the size range 0–0.5 mm, these are further grouped into three smaller size intervals, i.e. 0–0.1, 0.1–0.3, and 0.3–0.5 mm.

Because of the limited data available, the distribution of parameters in the proximate and ultimate analyses of the fuel is assumed to obey a known distribution, for example, a normal distribution. To simplify the model calculation, the coal particles are divided into two groups, i.e. ash-rich and ash-lean by dividing the normal distribution into two symmetrical halves at the mean value. Therefore, the mean ash content of these two groups of particles is the same as

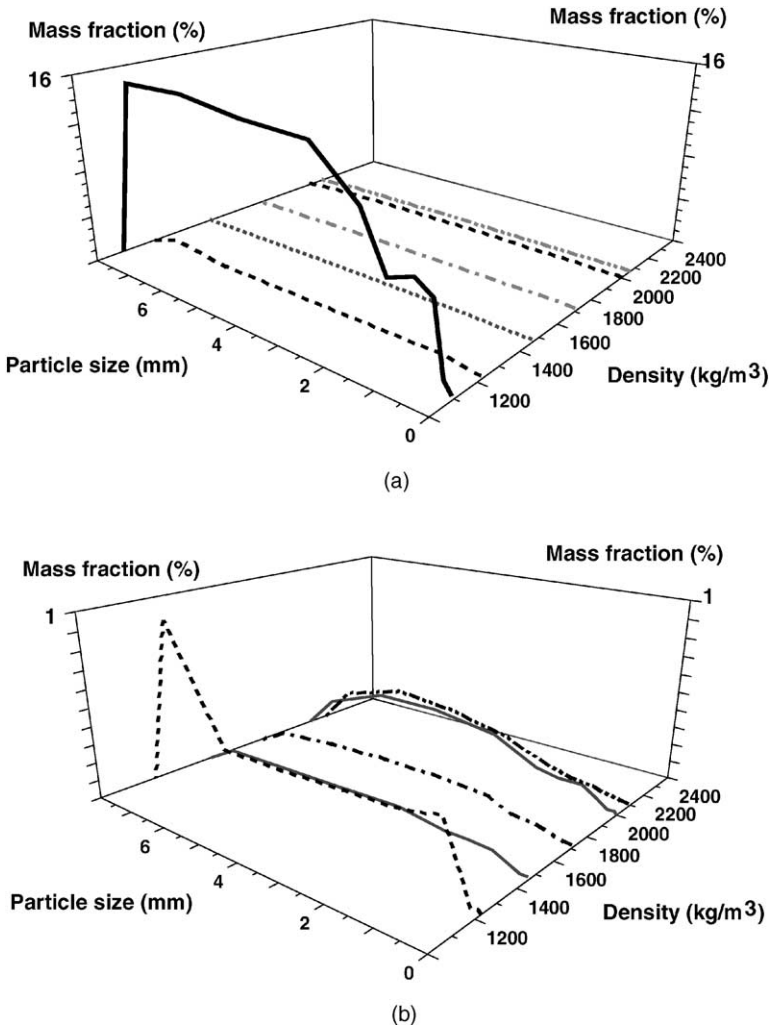

Fig. 3. (a–b) Particle population in the dense bed.

the measured ash content in the proximate analysis. For the cumulative normal distribution function of ash content $\phi(x)$ with a mean value of μ, parameter σ (standard deviation) may be specified to simultaneously satisfy the two following conditions: (1) $\phi(x = 0.5\mu) \approx 0.25$; (2) $\phi(x = 1.5\mu) \approx 0.75$. As the measured value of the ash content of the test coal is μ with a value of 23.7%, the average ash content of the ash-rich coal particles and the ash-lean coal particles are 35.6 and 11.8%, respectively. Similarly, other properties of the two groups of particles can be determined from the fuel analysis by specifying different σ.

The density of an ash-rich particle changes with time during combustion. The density of a spent ash particle with no carbon is the lowest, assuming 1100 kg/m^3. The average density of the char particle with no ash layer is the highest, assuming 2200 kg/m^3. Based on the carbon content, the density of the ash-rich char particles is divided into five classes from 1100 to 2200 kg/m^3, i.e. 1100–1105, 1105–1350, 1350–1595, 1595–1840, and 1840–2200 kg/m^3.

The coal particles with low ash contents burn in the single shrinking-core model, i.e. the particle average density keeping constant during combustion. Therefore, the average density of the ash-lean char particles can be treated as one group, assuming 2000 kg/m^3, and the fine ash particles generated from a burning ash-lean particle is assumed to have a density of 1100 kg/m^3. The other solid materials present in the furnace, such as limestone and inert bed materials can be considered as one group, assuming a density of 2400 kg/m^3.

The model input data are listed in Table 1 and compared with the measured parameters from the 12 MW CFB boiler. The feed water temperature was decreased to 105 °C from the designed value of 150 °C. Since the SO_2 emission is under the limit of the emission standard, no limestone is added to the furnace for sulfur retention.

Tables 2 and 3 show the ultimate and proximate analyses of the test coal and its size distribution, respectively.

The main calculation results are reported in the next section and compared with the measurement data. It should be noted that the measurement data for both the core and annulus regions are given as average values for the respective region.

5.1. Particle population in dense bed

Fig. 3 shows the particle population in the dense bed. Because no limestone and inert material were fed into the furnace, there are no particles with density $\rho = 2400$ kg/m^3. Since the mass fraction of each particle density class differs significantly from one another, the figure is divided into two parts, i.e. Fig. 3a for the particle groups with large mass fractions, and Fig. 3b for those with small mass fractions. It is shown in Fig. 3 that most of the bed materials in the dense bed are the coarse burnt-out ash particles with density between 1100 and 1105 kg/m^3. It implies that the carbon content in the dense bed is low. In addition, Fig. 3b shows that the mass fraction of the coarse char particles with a density

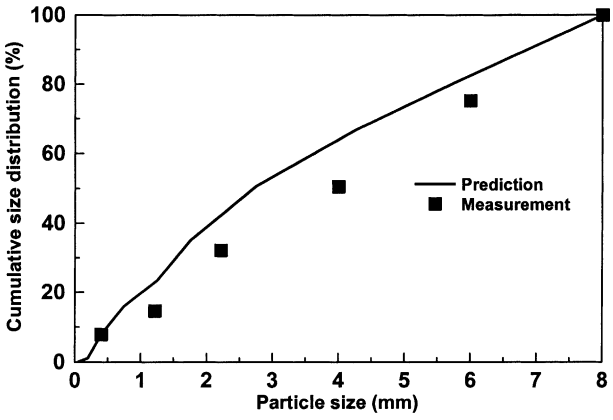

Fig. 4. Cumulative particle size distribution in the dense bed.

of 2000 kg/m^3 and the density range 1840–2200 kg/m^3 are higher than that of small size particles because only a small portion of the coarse char particles generated from devolatilization of fresh feed coal is entrained into the upper section of the furnace.

Fig. 4 shows the predicted particle size distribution in the dense bed. Despite the small deviation for coarser particles, the predictions are in substantial agreement with the experimental data.

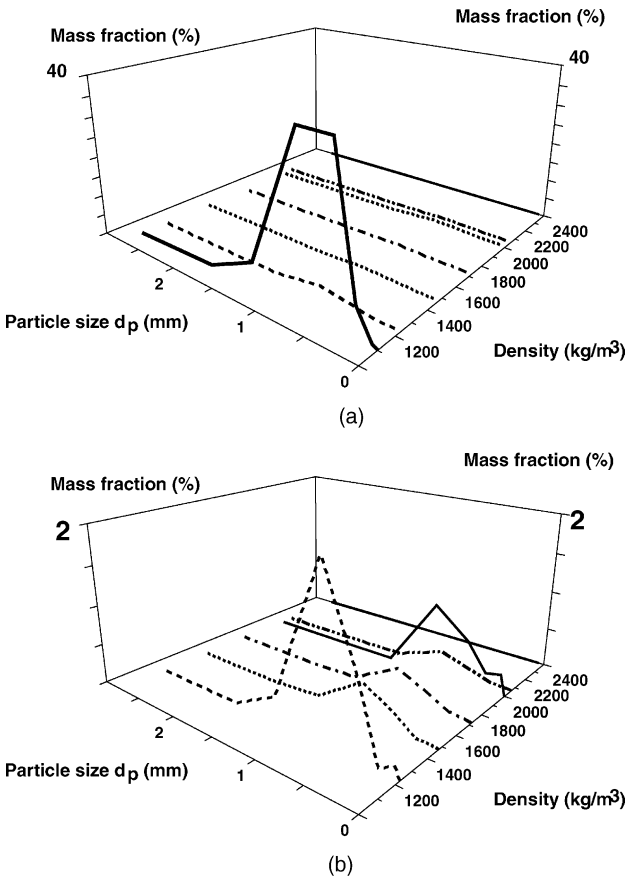

Fig. 5. (a–b) Population of particles at 13 m above distributor (core region).

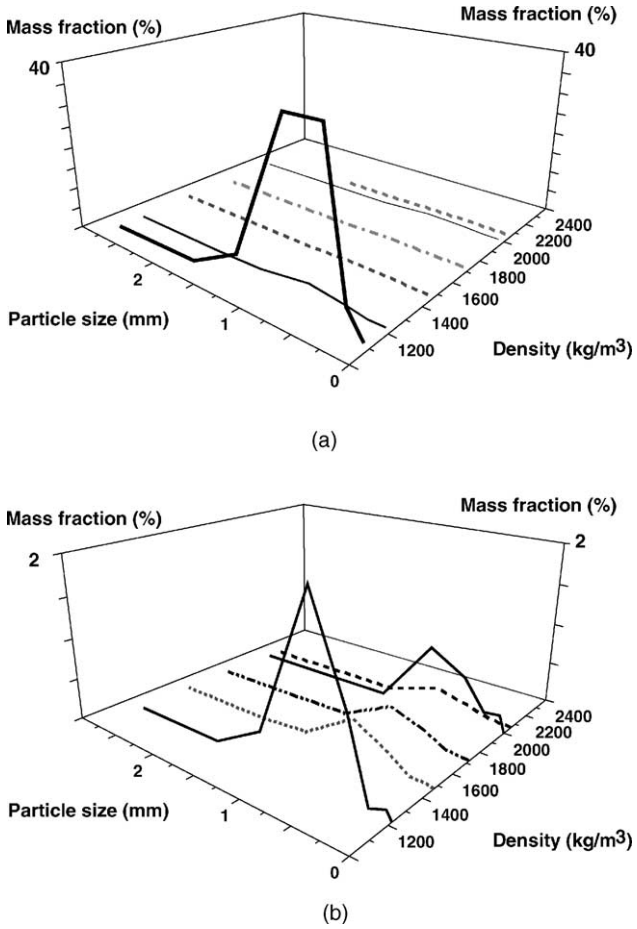

Fig. 6. (a–b) Population of particles at 13 m above distributor (annulus region).

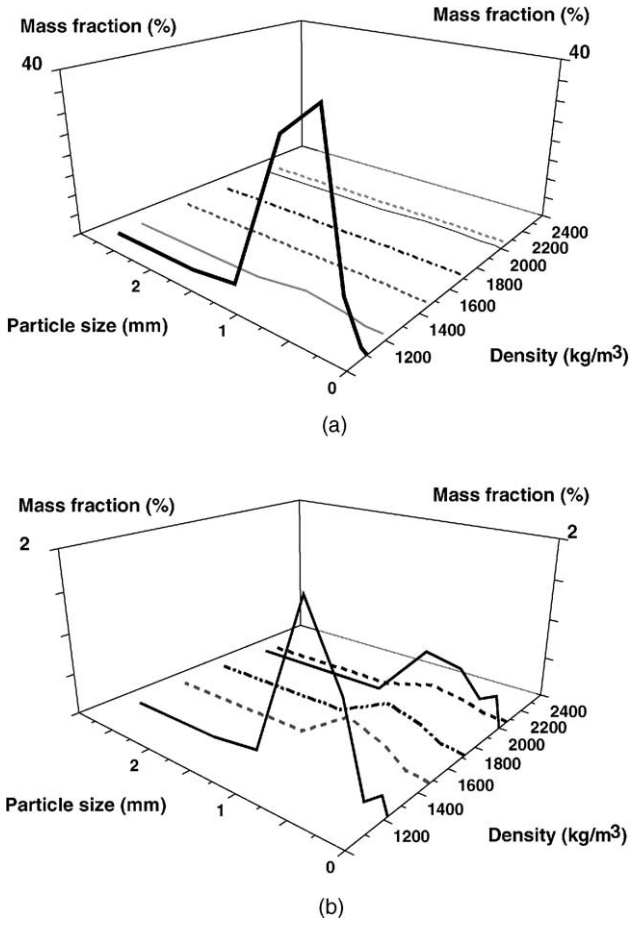

Fig. 7. (a–b) Population of particles at furnace exit.

5.2. Particle population in dilute region

The particle population distributions in the middle of the furnace (13 m above the distributor) and at the furnace exit are shown in Figs. 5–7, respectively. A systematic comparison is made in Figs. 8–10 between the predicted size distribution in the dilute region and the measured data. Most of the particles in the dilute region, with sizes in the range 0.2–1 mm, are also spent ash particles with low carbon content. The mass fraction of the ash-rich char particles increases with decreasing residual carbon content. This indicates that these ash-rich particles burn out progressively while circulating in the primary loop. In addition, Figs. 5 and 6 also show that the particle population distribution in the core region is similar to that in the annulus. Figs. 7 and 10 show that the particle size distribution at the furnace exit is also similar to that in the middle of the furnace, despite that the mass fraction of small particles is slightly greater at the furnace exit. As shown in Figs. 5b, 7b and 8b, small peaks appear in the size distribution densities corresponding to the size range 0–0.1 mm for particles with an average density of 2000 kg/m^3 and the density range 1100–1105 kg/m^3. This indicates that the fine particles come from both the spent ash and the char particles with high carbon content.

5.3. Particle population of fly ash

Fig. 11 shows the particle population distribution of fly ash. Fly ash consists of fine particles with a size of 0–0.1 mm. The mass fraction of ash-lean particles in this size range

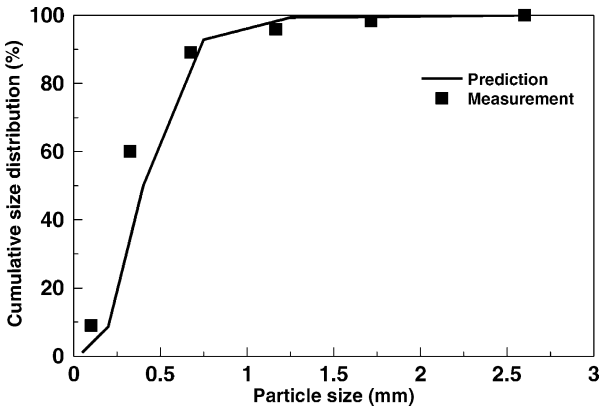

Fig. 8. Cumulative particle size distribution collected at 13 m above distributor (core region).

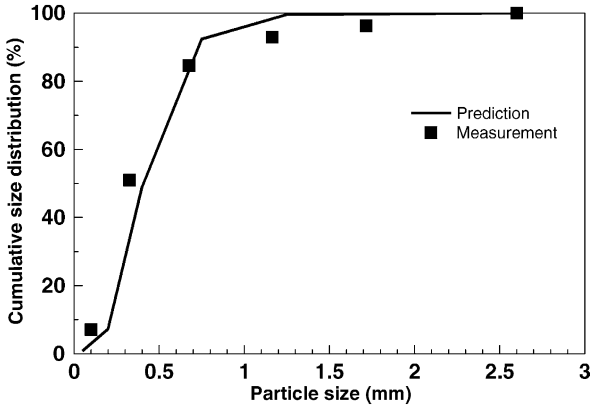

Fig. 9. Cumulative size distribution of particles collected at 13 m above distributor (annulus region).

($d_p = 0.05$ mm, $\rho = 2000$ kg/m^3) is about 13%, suggesting that this portion of particles cannot burn out after a single flight through the reaction zone. It is, therefore, attributable to a great portion of the unburnt carbon loss.

Fig. 12 compares the predicted size distribution of fly ash with the measured data. The predictions agree well with the experimental results.

5.4. Particle population along furnace height

The particle population balance varies along the height of the furnace. As shown in Fig. 13, the particle mean diameter decreases rapidly with increasing height in the furnace in both the core and the annulus regions, but only slightly in the upper furnace. It implies that the mass fraction of coarse particles decreases along the furnace height. The measurement data fit well to the predictions.

Fig. 13 again shows that the particle mean diameter in the core region is very close to that in the annulus region. The particle mean diameter in the core region is slightly smaller than that in the annulus except for the section 0–2 m above the dense bed. Many coarse particles are entrained into the dilute region and fall down to the dense bed, forming a solids reflux in the transport zone between the two parts of the furnace. Meanwhile, it is easier for the upflowing coarse particles to enter the low-velocity region. This explains why the mass fraction of the coarse particles near the wall is greater than in the core region.

The mass fraction of each group of particles varies in different ways along the furnace height. For the core region in particular, Fig. 14 shows the profiles of the mass fraction

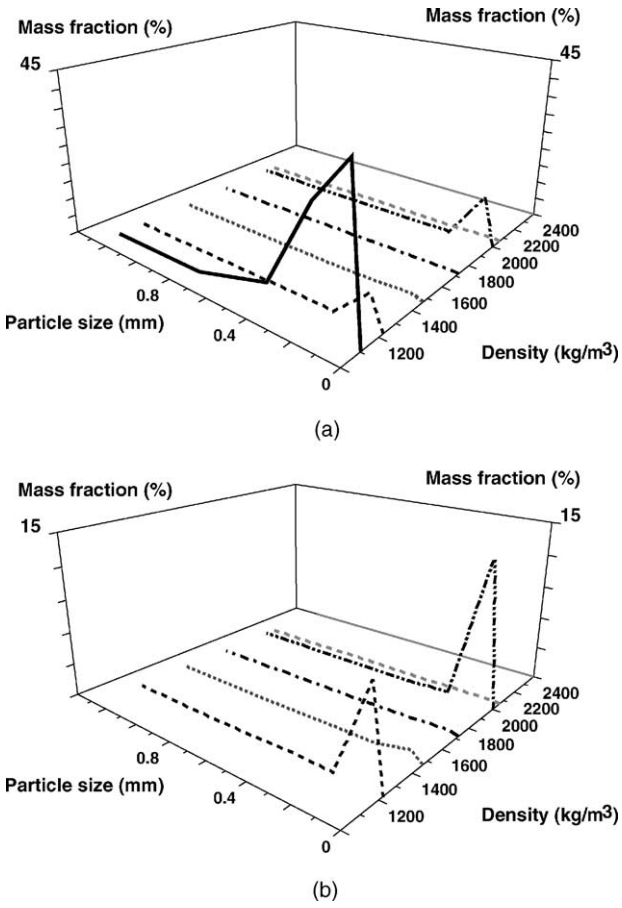

Fig. 11. (a–b) Population of fly ash particles.

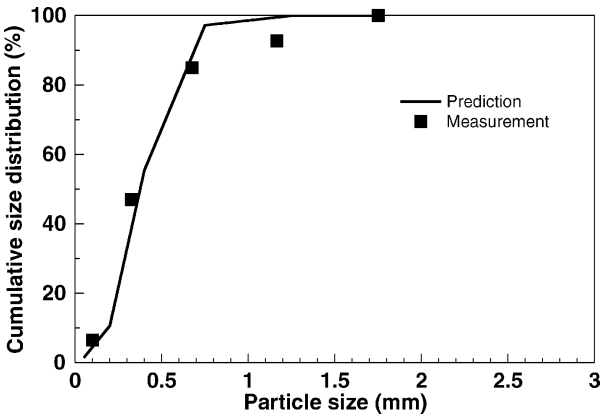

Fig. 10. Cumulative size distribution of particles collected at furnace exit.

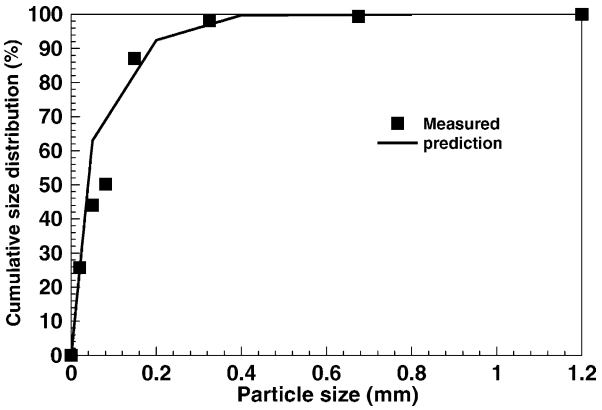

Fig. 12. Cumulative size distribution of fly ash.

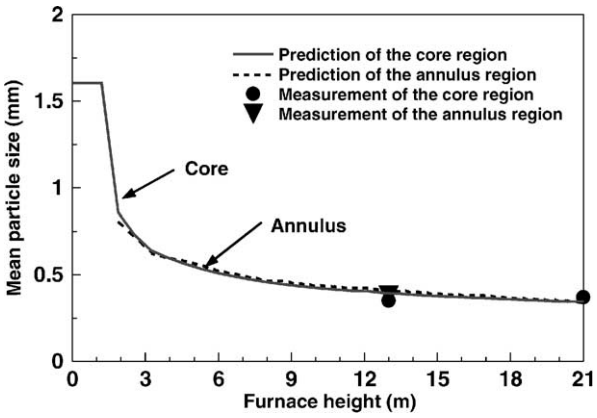

Fig. 13. Profile of particle mean diameter in furnace.

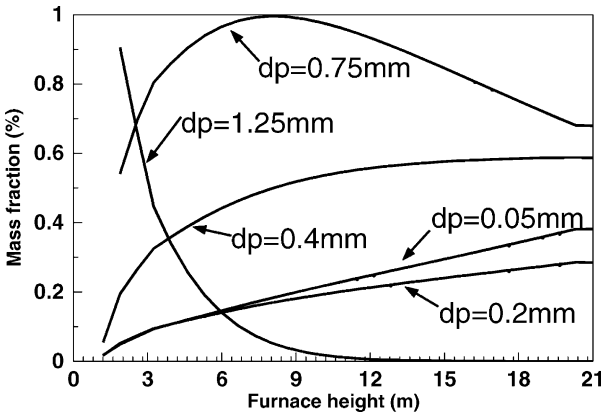

Fig. 15. Mass fraction profile of ash-lean particles ($\rho = 2000\,\mathrm{kg/m^3}$) along furnace height.

of the particle groups with the same size (0.3–0.5 mm) but different density along the furnace height. The profiles for the ash-lean particles ($\rho = 2000\,\mathrm{kg/m^3}$) are given in Fig. 15. The mass fraction of each particle group with a diameter of 0.3–0.5 mm increases along the furnace height, but levels off as particle density increases. However, not all particle groups increase their mass fractions with the furnace height. The fraction of coarse particles (>1 mm) decreases with the furnace height, while the fraction of medium size particles (0.5–1 mm) increases first and then decreases. One likely reason is that the coarse particles tend to migrate into the annulus region and fall down along the furnace wall. In addition, it seems that attrition of the ash-lean particles have a contribution to the significant increase in the mass fraction of fines with diameters in the range 0–0.1 mm (average d_p = 0.05 mm) along the furnace height shown in Fig. 15.

As shown in Fig. 15, some coarse particles, e.g. d_p = 1.25 mm, are only present in the lower part of the furnace. These particles are ejected from the dense bed but cannot be carried over to the upper furnace under the operating conditions examined.

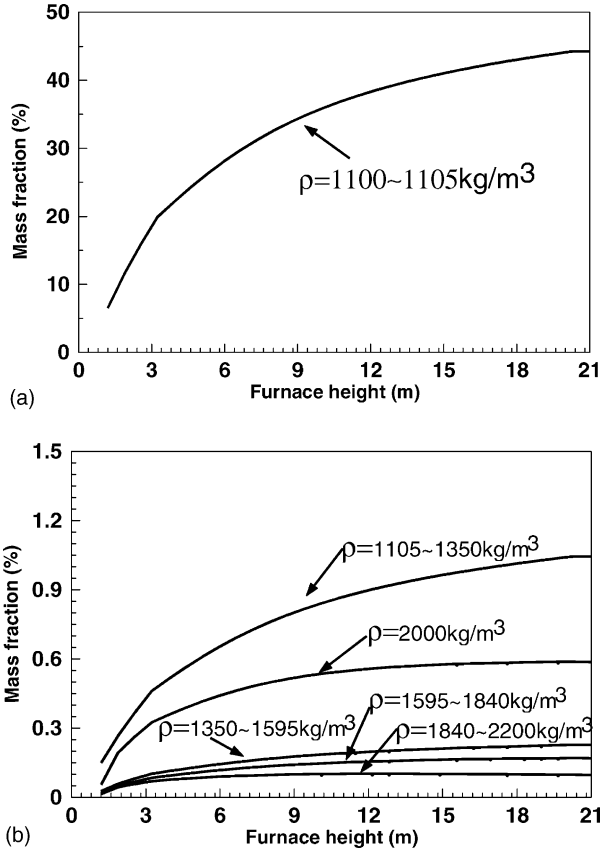

Fig. 14. (a–b) Mass fraction profile of the particles in the size range 0.3–0.5 mm along furnace height.

6. Conclusions

A particle population balance model for the CFB boiler furnace has been developed. The core–annulus model is employed to describe the hydrodynamics of the circulating fluidized bed furnace. The particles present in the CFB furnace are characterized and grouped by their size and density. The model considers particle fragmentation, char combustion, attrition and gas–solid separation. The model is integrated into a comprehensive model of a 12 MW CFB boiler developed earlier by the authors for performance prediction. The prediction results agree reasonably well with the measurement data.

Acknowledgements

The authors gratefully acknowledge the financial support from the Special Funds for China Major State Basic Research Projects (Grant G1999-022105).

References

[1] J.R. Grace, G. Sun, Influence of particle size distribution on the performance of fluidized bed reactors, Can. J. Chem. Eng. 69 (1991) 1126.

[2] M.L. Mastellone, U. Arena, The effect of particle size and density on solid distribution along the riser of a circulating fluidized, Chem. Eng. Sci. 54 (1999) 5383.
[3] D.R. Hajicek, M.D. Mann, T.A. Moe, A.K. Henderson, The effect of coal properties on CFBC performance, in: Lynn Rubow (Ed.), Proceedings of the 12th International Conference on Fluidized Bed Combustion, ASME, New York, 1993, p. 99.
[4] Y.C. Ray, T.S. Jiang, Particle population model for a fluidized bed with attrition, Powder Technol. 52 (1987) 35.
[5] Z. Li, W. Ni, G. Yue, Dynamic ash balance in circulating fluidized bed, J. Chin. Combust. Sci. Technol. 3 (1997) 258 (in Chinese).
[6] B.W. Overturf, G.V. Reklaitis, Fluidized-bed reactor model with generalized particle balances, AIChE J. 29 (1983) 813.
[7] J. Hannes, U. Renz, C.M. Van den Bleek, The IEA model for circulating fluidized bed combustion, in: K.J. Heinschel (Ed.), Proceedings of the 13th International Conference on Fluidized Bed Combustion, ASME, Orlando, 1995, p. 287.
[8] J. Adanez, L.F. de Diego, P. Gayan, L. Armesto, A. Cabanillas, Modelling of coal combustion in circulating fluidized bed combustors, in: K.J. Heinschel (Ed.), Proceedings of the 13th International Conference on Fluidized Bed Combustion, ASME, Orlando, 1995, p. 305.
[9] F. Bellgardt, F. Hembach, M. Schossler, J. Werther, Modeling of large scale atmospheric fluidized bed combustors, in: J.P. Mustonen (Ed.), Proceedings of the 9th International Conference on Fluidized Bed Combustion, ASME, Boston, 1987, p. 713.
[10] C.L. Senior, T. Zeng, J. Che, M.R. Ames, A.F. Sarofim, I. Olmez, F.E. Huggins, N. Shah, G.P. Huffman, A. Kolker, S. Mroczkowski, C. Palmer, R. Finkelman, Distribution of trace elements in selected pulverized coals as a function of particle size and density, Fuel Process. Technol. 63 (2000) 215.
[11] T.J. Pis, A.B. Fuertes, V. Artos, A. Suarez, F. Rubiera, Attrition of coal ash particles in a fluidized bed, Powder Technol. 66 (1991) 41.
[12] Y. Ray, T. Jiang, Particle attrition phenomena in a fluidized bed, Powder Technol. 49 (1987) 193.
[13] J. Werther, Fluid mechanics of large-scale CFB units, in: A. Avidan (Ed.), Circulating Fluidized Bed Technology IV, Pergamon Press, New York, 1994, p. 1.
[14] S.I. Plasynski, G.E. Klinzing, M. Mathur, High-pressure vertical pneumatic transport investigation, Powder Technol. 79 (1994) 95.
[15] D.R. Bai, Y. Jin, Z.Q. Yu, W.H. Yao, Two-channel model for fast fluidization, J. Chem. Ind. Eng. 1 (1990) 10 (in Chinese).
[16] J. Zhou, J.R. Grace, S. Oin, C.J. Lim, C.M.H. Brereton, Particle velocity profiles in a circulating fluidized bed of square cross-section, Chem. Eng. Sci. 50 (1995) 237.
[17] W.N. Zhang, F. Johnsson, B. Leckner, Fluid-dynamic boundary layers in CFB boilers, Chem. Eng. Sci. 50 (1995) 201.
[18] J. Bi, G. Yang, T. Kojima, Lateral mixing of coarse particles, Trans. IChemE 73 (1995) 162.
[19] G.S. Patience, J. Chaouki, Kennedy, Solids residence time distribution in CFB reactors, in: P. Basu, M. Horio, M. Hasatani (Ed.), Circulating Fluidized Bed Technology III, Pergamon Press, New York, 1991, p. 599.
[20] M.J. Rhodes, S. Zhou, S. Hirama, H. Cheng, Effects of operating conditions on longitudinal solids mixing in a circulating fluidized bed riser, AIChE J. 37 (1991) 1450.
[21] L.D. Smoot, P.J. Smith, Coal Combustion and Gasification, Plenum Press, New York, 1985.
[22] R. Chirone, L. Massimilla, P. Salatino, Comminution of carbon in fluidized bed combustion, Prog. Energy Combust. Sci. 17 (1991) 297.
[23] U. Arena, A. Cammarota, L. Massimilla, L. Siciliano, P. Basu, Carbon attrition during the combustion of a char in a circulating fluidized bed, Combust. Sci. Technol. 73 (1990) 383.
[24] S.T. Pemberton, J.F. Davidson, Elutriation from fluidized beds. I. Particle ejection from the dense phase into the freeboard, Chem. Eng. Sci. 41 (1986) 243.
[25] K. Cen, M. Ni, Z. Luo, J. Yan, Y. Chi, M. Fang, X. Li, L. Cheng, Circulating Fluidized Bed Boiler—Theory, Design and Operation (in Chinese), China Electric Press, Beijing, 1998, p. 95.
[26] Q.H. Wang, Mathematical modeling and performance testing of circulating fluidized bed boiler, Ph.D. Thesis, Zhejiang University, Hangzhou, China, 1997.
[27] Q.H. Wang, Z.Y. Luo, X.T. Li, M.X. Fang, M.J. Ni, K.F. Cen, A mathematical model for a circulating fluidized bed, Energy 24 (1999) 633.